PAPER

Experimental and numerical study on the influence of flow passages in centrifugal fan using computational fluid dynamics

Engineering Research Express

PAPER

Experimental and numerical study on the influence of flow passages in centrifugal fan using computational fluid dynamics

RECEIVED
19 January 2023

REVISED
31 March 2023

ACCEPTED FOR PUBLICATION
20 April 2023

PUBLISHED
11 May 2023

Viral Kumar Patel Babubhai[1], **Abhimanyu Chaudhari**[2,*], **Ashwani Sharma**[2] and **Vikas Diwakar**[2]

[1] Research and Development (Air compressor Division), Kirloskar Pneumatic Company Limited, Pune - 411013, Maharashtra, India
[2] Department of Mechanical Engineering, Indian Institute of Technology (Banaras Hindu University), Varanasi - 221005, Uttar Pradesh, India
[*] Author to whom any correspondence should be addressed.

E-mail: VIRALKUMAR.Patel@kirloskar.com, abhimanyuchaudhari.rs.mec18@iitbhu.ac.in, ashwanisharma.rs.mec18@iitbhu.ac.in and vikasdiwakar.rs.mec21@iitbhu.ac.in

Keywords: computational fluid dynamics, mass flow rate, impeller blade, centrifugal fans

Supplementary material for this article is available online

Abstract

In this work, three actual impeller geometries of identical size, with backward, radial, and forward flow passages in the same volute casing, are experimentally analysed and numerically simulated to understand the flow physics characteristics and the performance mapping under different flowrate conditions. A grid independence test is carried out for the whole computational domain to capture complex flow behaviour inside blades. The three-dimensional numerical analysis is performed under steady flow conditions, and for a rotational domain, a moving reference frame approach (frozen rotor method) is used. The results obtained from experimental and simulated cases for backward, radial, and forward curved centrifugal fans with varying mass flowrates shows that static pressure and total pressure are increased with an increase in rotation speed and the static pressure gradient is higher in forward curved blades than in backward and radial bladed centrifugal fans. A blade's low and high-pressure regions along the suction and pressure sides are visualised by numerical analysis. The degree of recirculation within blade passages, flow reversal and vortex formation in volute and tongue regions is observed to be different in all three types of flow passages, which clearly describes its influence on the performance characteristics of centrifugal fans.

1. Introduction

Centrifugal fans have been extensively used in a wide range of engineering applications, including the automobile industry to cool internal combustion engines; central heating and cooling systems in buildings; cupola fans; blast furnace gas fans; water gas fans; municipal gas plant fans; coke plant exhausters; agricultural works; and aeroplane superchargers [1–3]. It is one of the power-consuming turbo machines, requiring large volumes of gas or air at low pressures. The pressure ratio of compressed air varies from 1 to 1.11 [4]. It consists of an impeller rotating in a stationary casing having a spiral shape. The air enters in the impeller axially and leaves in a radial direction, and the same fluid is collected in a casing. Impeller blades impart energy to the fluid. There are three main blade profiles: backward-curved, radial-tipped, and forward-curved. Despite little compression in the impeller and fan, the air in fans is usually considered incompressible [5]. The pressure developed by a fan depends on the volume flow of air. As the volume flow decreases, the fan pressure increases, reaching a maximum value at a point in the range of volume flow depending on the particular design of a fan. The pressure developed also increases with an increase in blade angle, impeller speed and the number of blades up to a specific limit. An increase in the number of blades in an impeller makes the passage narrower, giving better guidance to the fluid and reducing the circulatory flow effect. However, it increases resistance to flow, profile loss, and reduction in flow area, so the amount of volume flow will decrease [6]. The performance of any fan is measured in terms of pressure, volume flow, and power absorbed. This depends upon the following variables: the design

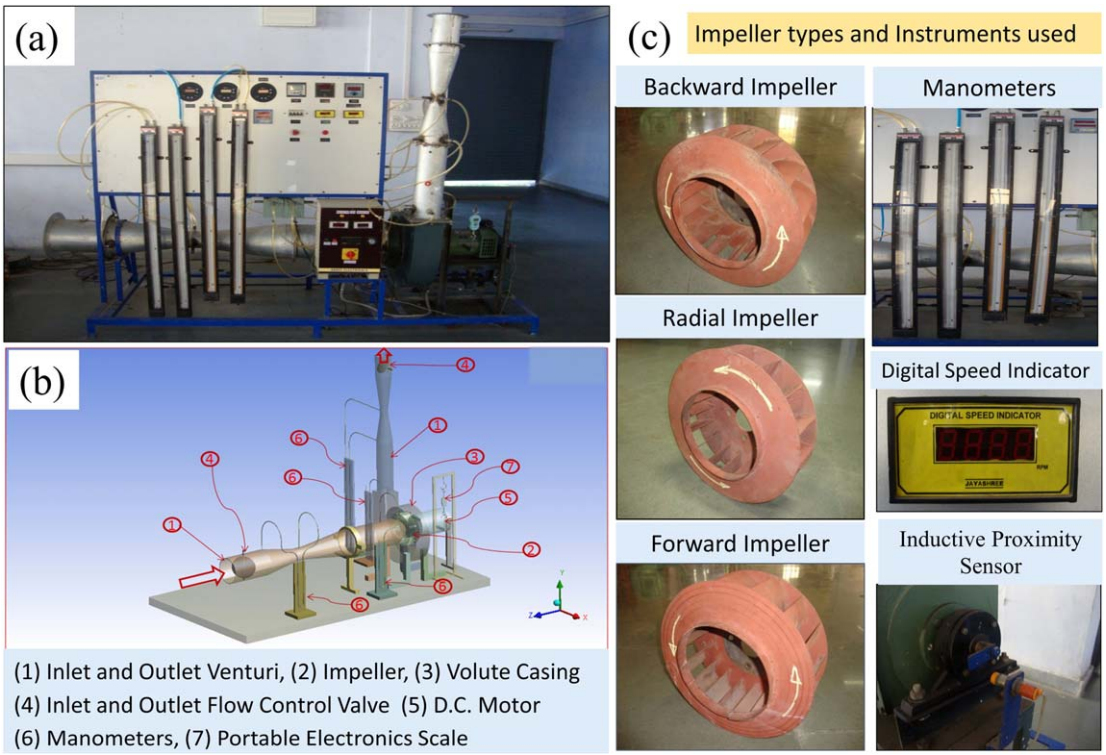

Figure 1. (a) Actual experimental setup, (b) 3-D Model of experimental layout, (**c**) Parts of setup.

and type of fan; the point of operation on the volume flow/pressure characteristic curve; the size of the fan; the speed of rotation of the impeller; and the condition of the air or gas passing through the fan [7]. Numerous in-depth experiments have been conducted to comprehend the flow within centrifugal fans. Wright *et al* [8] demonstrated that moderate to severe distortion of inflow patterns can cause a significant reduction in efficiency and pressure rise, up to 10%–15%. Inlet distortion can lead to partial flow separation at the fan entrance compared to non-distorted conditions, and the flow range becomes narrower. This is because seriously distorted inflows can affect the onset of flow instability, such as rotating stall and surge, in centrifugal fans. Lei *et al* [9] stated that when the flow rate is 4.30 m3/s, the original fan experiences a rotating stall, with the onset of the stall occurring initially in three impeller passages near the volute tongue and front disc. The influence of various blowing speeds (50, 70, 90, 110, and 130 m s^{-1}) was analyzed during the stall's initiation. They found the optimal blowing speed for inhibiting stall inception at 110 m s^{-1} blowing speed. Choi *et al* [10] conducted numerical simulations of the stall and compared the results with experimental data obtained at two different fan speeds. The findings indicated that the stall characteristics closely corresponded to the experimental data. Bhope and Padole [4] conducted a study on the fluid flow within the impeller of a centrifugal fan. They noted that incorporating a stiffening ring caused a slight decrease in both air pressure and airflow. However, this reduction could be easily counterbalanced by running the impeller at a slightly higher speed, without compromising its strength and stiffness. Due to the following flow characteristics: separation, reverse and secondary flows, turbulent flow, boundary layer effects, and compressibility effects, making a proper experimental assessment of turbomachines is difficult [11, 12].

Recent advances in computing power, with powerful graphics and interactive 3D manipulation of models, have made creating a computational fluid dynamics (CFD) model and analysing results much less labour-intensive, reducing time and cost [13, 14]. Advanced solvers contain algorithms that enable robust flow field solutions in a reasonable time. Bhatti *et al* [15] reported that various flow phenomena occurring inside turbomachines can be numerically analysed with the help of commercially available CFD software. Nowadays, three-dimensional flow calculations are feasible, allowing designers to estimate more accurately the influence of spatial flow non-uniformity on machine performance [16, 17]. According to the Moczko *et al* [18], the calculation was carried out utilizing the 'frozen rotor method' and appropriate expressions that account for the impact of centrifugal forces while the impeller is rotating. Any realistic flow simulation must be done on a three-dimensional basis. Due to the curved passages inside the impeller and the volute, the flow is considered three-dimensional. The set of equations which describe the processes of momentum, heat, and mass transfer is known as the Navier–Stokes equations [19].

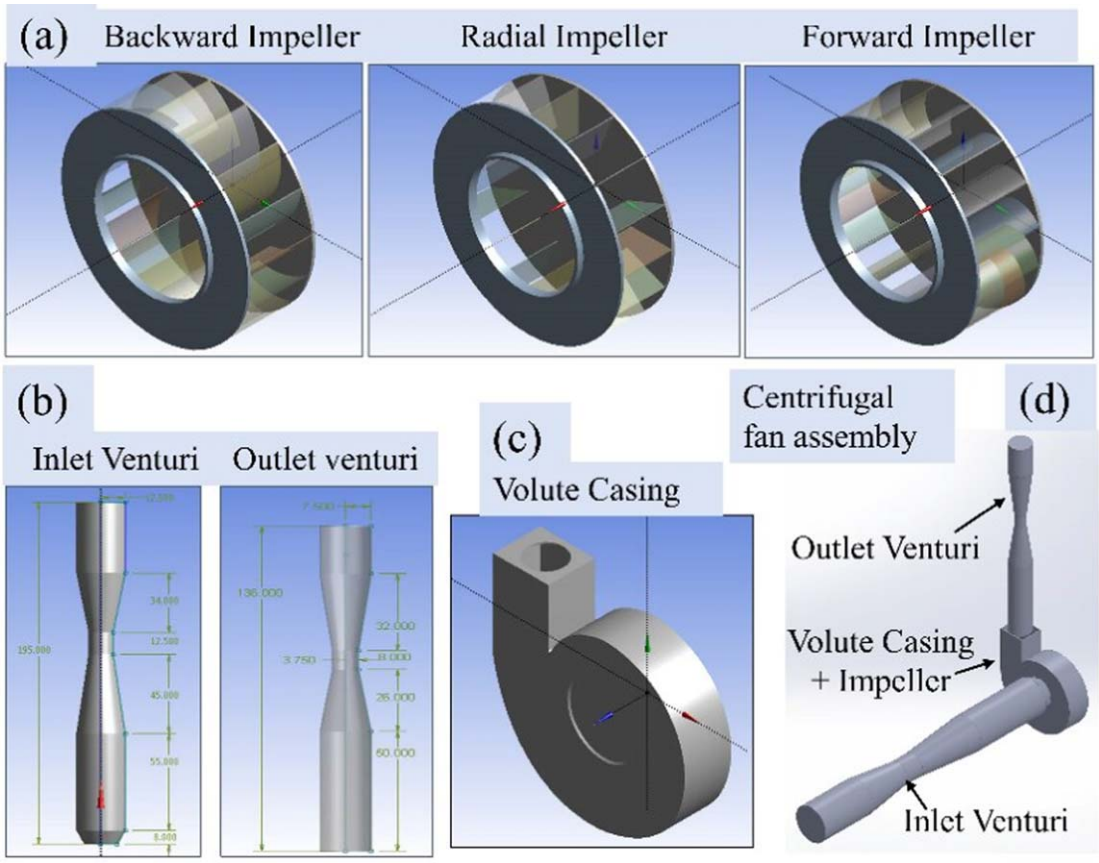

Figure 2. Various component and assembly of centrifugal fan.

Table 1. Dimension specification of impeller.

Parameter	Backward blade dimension	Radial blade dimension	Forward blade dimension
Inlet Diameter (cm)	19	19	19
Outlet Diameter (cm)	32	33.5	32
Inlet Blade Angle (degree)	60	90	70
Outlet Blade Angle (degree)	34	90	154
Thickness of Blade (mm)	2	2	2
Number of Blades	16	16	16
Width of Blade (cm)	10.5	8.5	10.5

Table 2. Dimension specification of volute casing.

Parameter	Dimension
Volute base circle diameter (cm)	32
Volute exit diameter (cm)	65
Volute width (cm)	15
Tongue angle (degree)	17
Tongue radius (cm)	13.975

Flow physics governs the performance of a centrifugal fan. The principal focus of the present work is to understand the flow behaviour in flow passages of three nearly readily available impeller geometries, i.e., backward, radial, and forward-curved blades. Three nearly identical-sized impellers with backward, radial, and forward blades are numerically analysed with the commercially available software ANSYS CFX 21. The volute configuration is kept the same in all three cases to obtain a discernible influence from the flow passages in the centrifugal fan. The numerical results are validated through experiments under varying mass flow rates conditions. The performance that has been seen is linked to the flow physics that has been found through

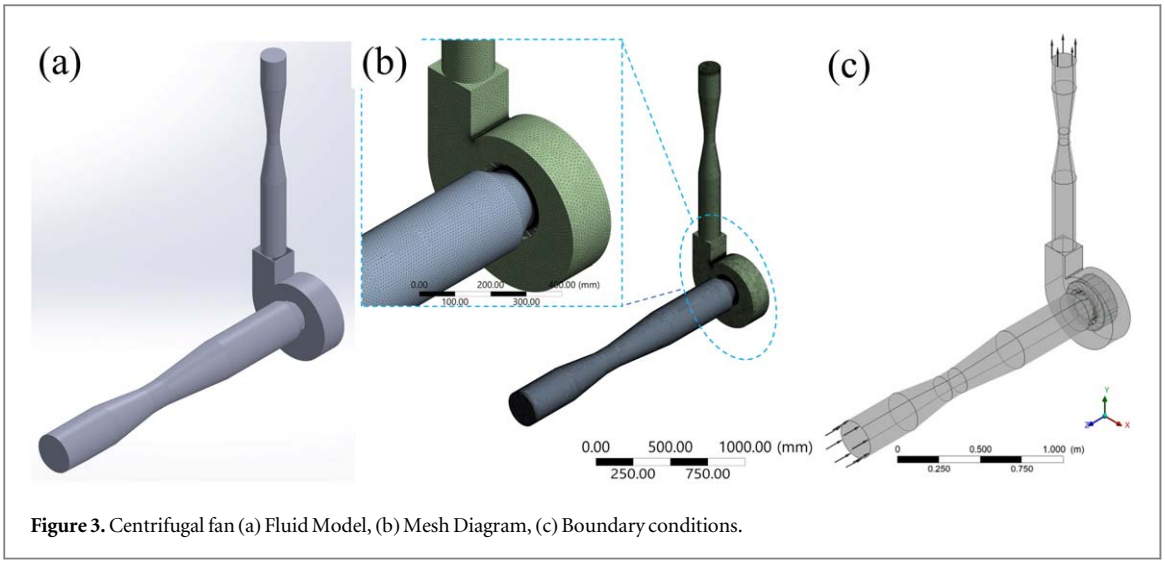

Figure 3. Centrifugal fan (a) Fluid Model, (b) Mesh Diagram, (c) Boundary conditions.

Table 3. Profile points of backward blade by point-by-point method.

R	β	$\tan\beta$	$\frac{1}{R\tan\beta}$	$\left(\frac{1}{R\tan\beta}\right)_{avg}$	ΔR	$\Delta R\left(\frac{1}{R\tan\beta}\right)_{avg}$	$\Delta\theta$	θ
9.5	60	1.730	0.061	0.063	0.500	0.031	1.792	0.000
10	57.318	1.557	0.064	0.065	0.500	0.033	1.865	1.792
10.5	55.351	1.445	0.066	0.067	0.500	0.033	1.913	3.657
11	53.384	1.344	0.068	0.069	1.000	0.069	3.984	5.571
12	49.45	1.168	0.071	0.073	1.000	0.073	4.213	9.554
13	45.516	1.017	0.076	0.078	1.000	0.078	4.476	13.767
14	41.582	0.887	0.081	0.084	1.000	0.084	4.788	18.243
15	37.648	0.771	0.086	0.088	0.500	0.044	2.528	23.031
15.5	35.681	0.718	0.090	0.092	0.500	0.046	2.632	25.559
16	33.714	0.667	0.094					28.190

Table 4. Profile points of forward blade by point-by-point method.

R	β	$\tan\beta$	$\frac{1}{R\tan\beta}$	$\left(\frac{1}{R\tan\beta}\right)_{avg}$	ΔR	$\Delta R\left(\frac{1}{R\tan\beta}\right)_{avg}$	$\Delta\theta$	θ
9.5	70	2.742	0.038	0.031	0.500	0.016	0.896	0
10	76.461	4.141	0.024	0.018	0.500	0.009	0.517	0.896
10.5	82.922	8.006	0.012	0.006	0.500	0.003	0.186	1.413
11	89.384	86.635	0.001	−0.009	1.000	−0.009	−0.489	1.598
12	102.30	−4.604	−0.018	−0.027	1.000	−0.027	−1.555	1.110
13	115.23	−2.128	−0.036	−0.046	1.000	−0.046	−2.641	−0.445
14	128.15	−1.276	−0.056	−0.069	1.000	−0.069	−3.965	−3.086
15	141.07	−0.810	−0.082	−0.092	0.500	−0.046	−2.629	−7.051
15.5	147.53	−0.638	−0.101	−0.114	0.500	−0.057	−3.279	−9.680
16	154	−0.489	−0.128					−12.95

Table 5. Simulation parameters used in solver.

Parameters	Conditions
Inlet boundary condition	Static pressure in Pa
Outlet boundary condition	Mass flow rate in kg/s
Inlet duct and impeller interface domain	Frozen rotor
Impeller and casing interface domain	Frozen rotor
Numbers of mesh elements	750893
Speed of impeller	2800 RPM
Turbulence Model	K-epsilon (k-ε)

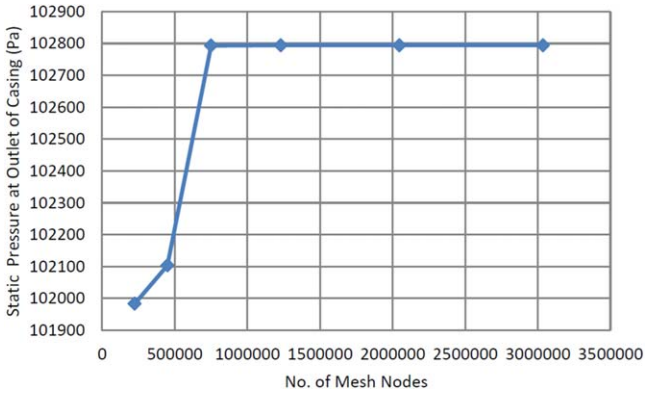

Figure 4. Grid independency test.

Table 6. Grid independency test.

Mesh name	No. of Mesh nodes	Static pressure at outlet of casing (Pa)	Static pressure difference at casing (Pa)	Pressure ratio
a	224726	101983	855	1.008447
b	450367	102103	975	1.009633
c	750893	102793	1665	1.016456
d	1230580	102794	1666	1.016466
e	2046350	102794	1666	1.016466
f	3035848	102794	1666	1.016466

numerical simulation for each type of flow passage and makes a comparative assessment of numerical and experimental studies.

2. Experimental procedure

The experimental setup available at SVNIT, Surat, Boiler Laboratory Extension was modified accordingly and fully instrumented to study the flow characteristics of a centrifugal fan with three different impellers, backward, radial, and forward, with the same volute casing. The details of the experimental setup, a 3-D CAD model with impeller types and instruments, are shown in figures 1(a)–(c). In this present study, all experiments are carried out at atmospheric pressure and temperature. The air enters the impeller axially through the nozzle, which provides slight acceleration to the air before it enters the impeller. The action of the impeller swings the air from a smaller to a larger diameter of the impeller with centrifugal action and delivers it to the casing at a slightly higher pressure and velocity. The flow is collected by a spiral-shaped casing called a volute. Flow coming out of the impeller is collected in the volute casing. In the casing, static pressure increases and velocity decreases with an increase in area, and then flow goes to the outlet duct. The butterfly valve shuts off the air. They are 100% tight in the closed position, streamlined versions of the disc that prevent turbulence, and service-free. Figure 1(b) shows two valves at the beginning of the inlet venturi and at the end of the outlet venturi, respectively. A single-stage centrifugal fan is run by a D.C. motor with a capacity of 3 hp and a maximum rotational speed of 3000 rpm. Using the speed regulator, the speed of the motor varies, and the variable-speed flow of the centrifugal fan also varies. In the experiment, air velocity at the inlet and outlet is calculated from the venturi. For the calibration of the venturi, a reading anemometer was used. It measures the velocity range from 0 to 30 m/s with an accuracy of 2%.

To measure air volume flow rate, two venturis are placed at the inlet and outlet of the volute casing with a manometer, as shown in figure 1. The equation (1) used for the measurement of flow is:

$$Q = \frac{C_d A_2}{\sqrt{1-\beta^4}} \sqrt{2gH_{mf}\left(\frac{\rho_{mf}}{\rho_a} - 1\right)} \tag{1}$$

Where, Q: volumetric flow rate in m^3/s; C_d: coefficient of discharge; A_2: area at throat in m^2;

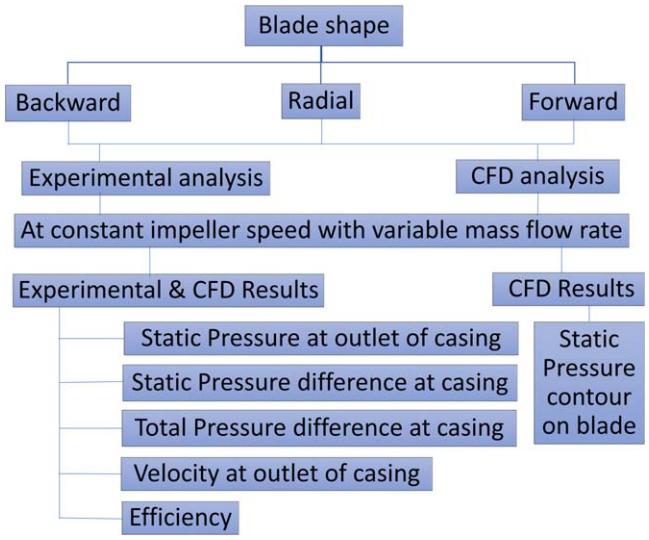

Figure 5. Flow diagram for different cases analysed during experimental and CFD studies.

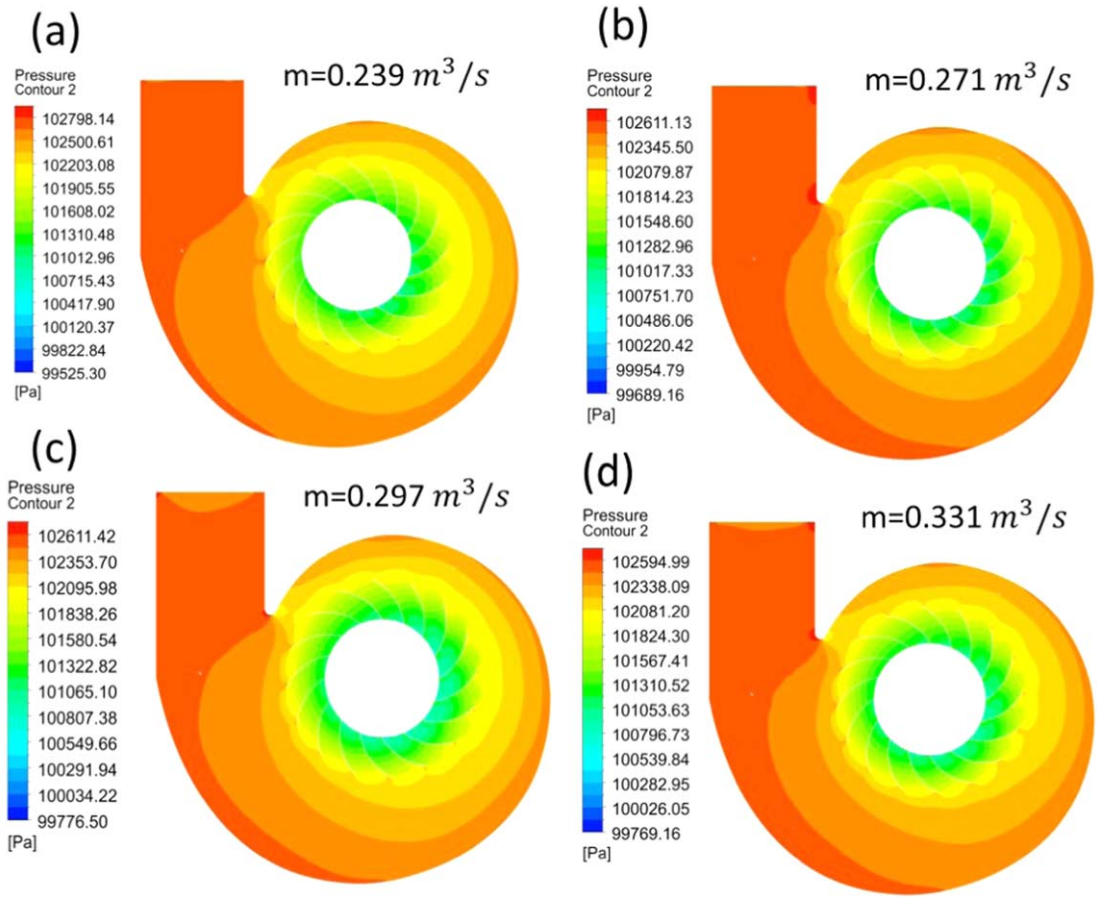

Figure 6. Static pressure contours at mid plane of casing for backward blade with variable mass flowrate.

B: d/D; d: diameter at throat of venturi in m; D: diameter at inlet if venturi in m; H_{mf}: manometric pressure difference in m of water; ρ_{mf}: density of water in m^3/s; ρ_a: density of air in m^3/s.

At the inlet and outlet of the casing, pressure is measured with the two separate U-tube manometers, and water is used as the manometric fluid. It ranges from 0 to 120 cm of water, and the minimum value of the manometer reading is 1 mm of the water column. D.C. motor speed is measured with the help of a digital speed indicator with a minimum accuracy of around 1 rpm (refer to figure 1). At the open end of the motor shaft, one metal strip is fixed and rotates with it. The inductive proximity sensor senses the metal strip when the motor

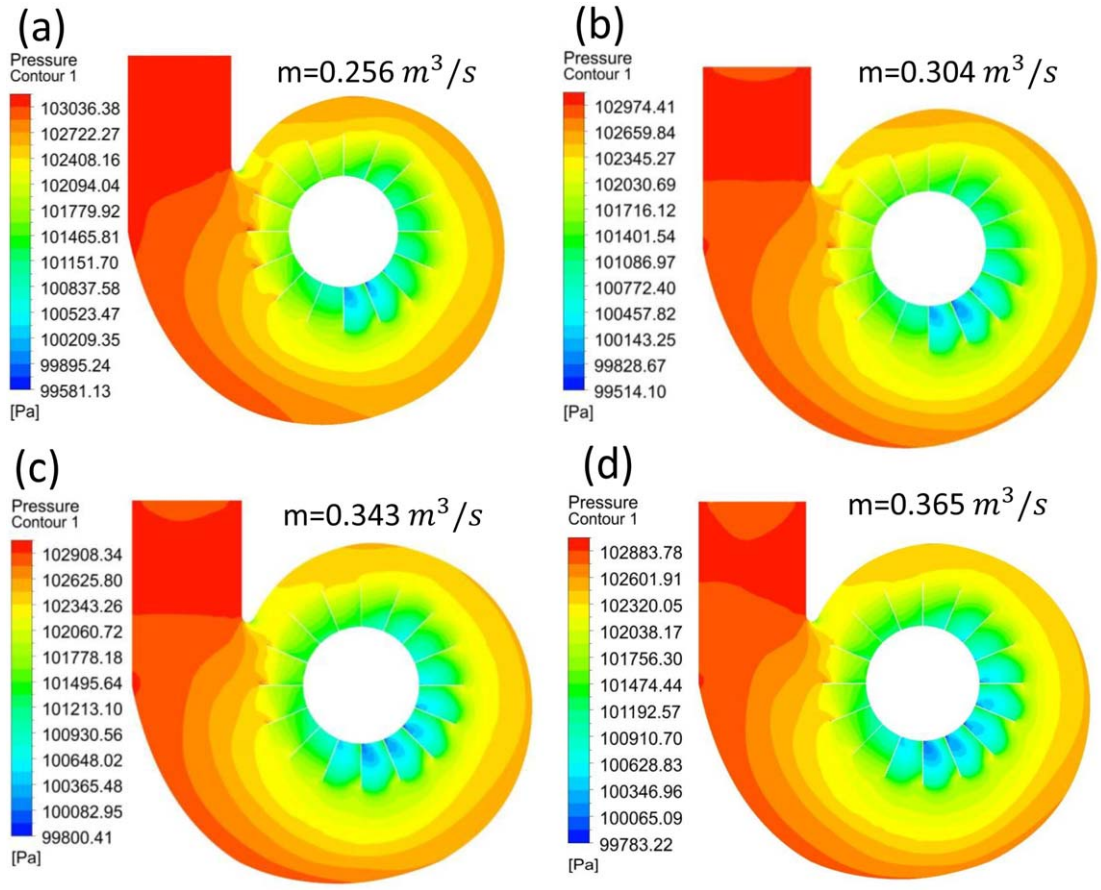

Figure 7. Static pressure contours at mid plane of casing for radial blade with variable mass flowrate.

rotates, and its signal transfers to the digital speed indicator. As shown in figure 1, a portable electronic scale is mounted on the motor to measure the D.C. motor's torque. When the motor rotates, the motor generates a tangential force on the portable electronic scale and shows a reading in the kg unit. It measured a maximum weight of up to 40 kg and a minimum weight of 10 g. The thermometer is used to measure atmospheric temperature based on which the density of air is calculated, and it is used in calculating air mass flow rate.

A leakage test is conducted to ensure the casing and outlet ducts are not leaking. First, start the centrifugal fan and check for leakages with the help of the soap bubble test. This test is done with great care, and if any leaks are found, the right steps are taken to fix them. System calibration is an essential prerequisite for any experiment. There are several reasons why an observed reading deviates from a set or calibrated value. It is assumed that this shift or deviation from the standard or calibrated value is constant and is the basis for any instrument. In our case, two instruments that need calibration are a portable electronic scale and a digital speed indicator. A portable electronic scale is used to measure the torque of the motor. It shows the reading in terms of kg. So, it is calibrated with the help of a known weight. In our case, it is checked with the help of a 1 kg standard weight. A digital speed indicator is used to measure the speed of the motor. It is calibrated with the help of a digital tachometer with an accuracy of 1 rpm. Each experiment group was run with three repetitions to reduce random test errors, and the average value was calculated.

3. Computational methodology modeling approach

3.1. Creating the geometry and mesh

This interactive process is the first pre-processing stage. The objective is to produce a mesh for input to the physics pre-processor. Before a mesh can be produced, a closed geometric solid is required. The Solidworks software was used to design, modelled, and assemble different components of the centrifugal fan, as shown in figure 2. The dimension specification of the impeller and volute casing is shown in tables 1 and 2, respectively. The blade profile was obtained using the point-by-point method [20]. The detailed calculations of blades profile coordinates are summarized in table 3 and 4. Further defining the geometry of region of interest. After that,

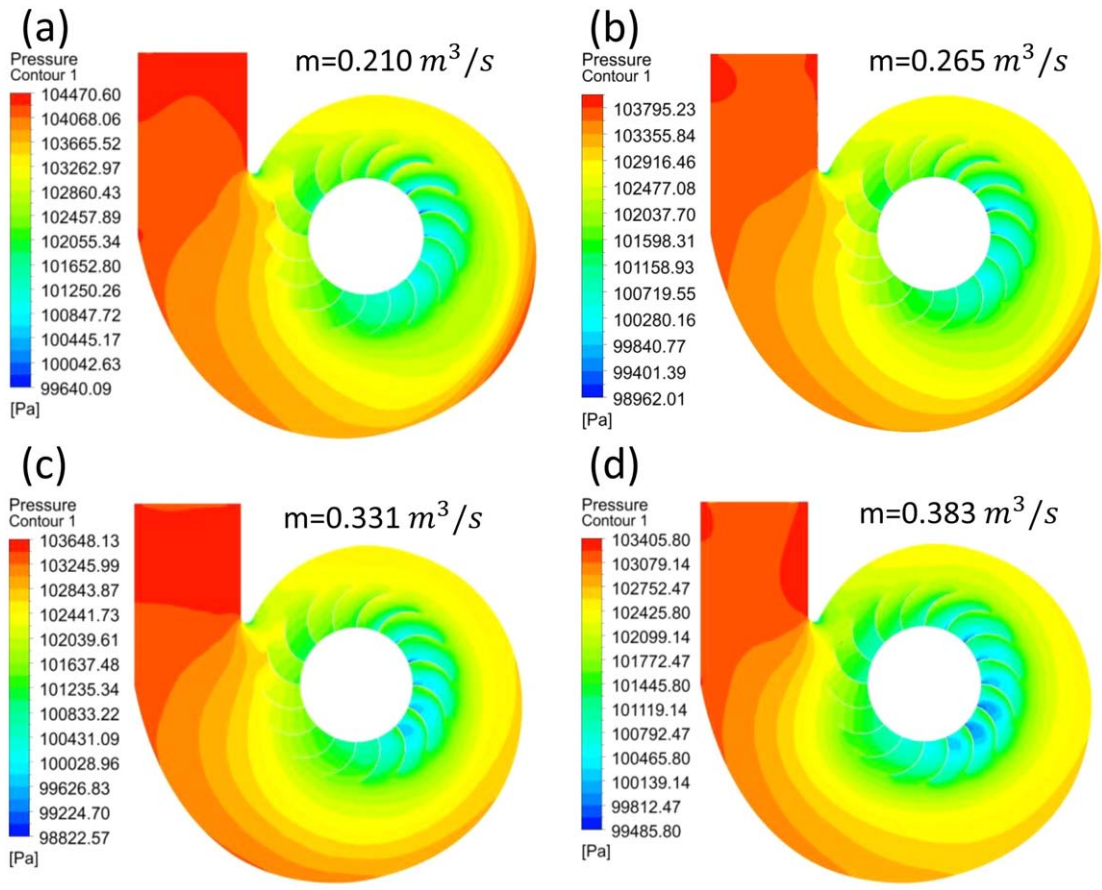

Figure 8. Static pressure contours at mid plane of casing for forward blade with variable mass flowrate.

create fluid flow regions, solid regions, and surface boundary names. The next step was to set properties for the mesh, as shown in figure 3.

3.2. Defining the physics of the model

This interactive process is the second pre-processing stage and is used to create the input required by the Solver. The mesh files are loaded into the physics pre-processor, CFX-Pre. The physical models that are to be included in the simulation are selected. The boundary conditions used in the simulations were as follows: a steady-state inlet condition was applied to the impeller blade passages, and a mass flow rate boundary condition was applied to the outlet of the fan. The walls of the impeller blades and volute casing were treated as no-slip boundaries, and a near-wall treatment was applied to the wall cells to capture the boundary layer effects accurately. Also, table 5 indicated the initial boundary condition used during the simulation. To ensure the accuracy of the developed model, a convergent graph is made between the static pressure at the outlet and number of the mesh nodes present which is shown in the figure 4. The component that solves the CFD problem is called the Solver. It produces the required results in a non-interactive batch process. The partial differential equations that solve a CFD problem are integrated over all the control volumes in the region of interest. This is the same as applying a fundamental mass or momentum conservation law to each control volume.

3.3. Grid independency test

The meshing of all zones was done by unstructured mesh using quad and tri elements. The mesh resolution was refined near the walls of the impeller blades and volute casing, where the flow gradients were high. The mesh was also refined in the impeller blade passages, where the flow was complex and unsteady. The mesh refinement was achieved using a local mesh refinement technique, which automatically refined the mesh in regions of high flow gradients. To optimise the number of grids and to develop grid independency, first very coarse grids were generated and then, by successively decreasing the size of mesh elements, the obtained results were evaluated. To get better grid independence, the chosen parameters are changes in static pressure across the fan, static outlet pressure, and the overall pressure ratio of the fan. Results obtained for the above-stated parameters under the varied number of total elements are presented in table 6. A graphical representation in figure 4 also presents it.

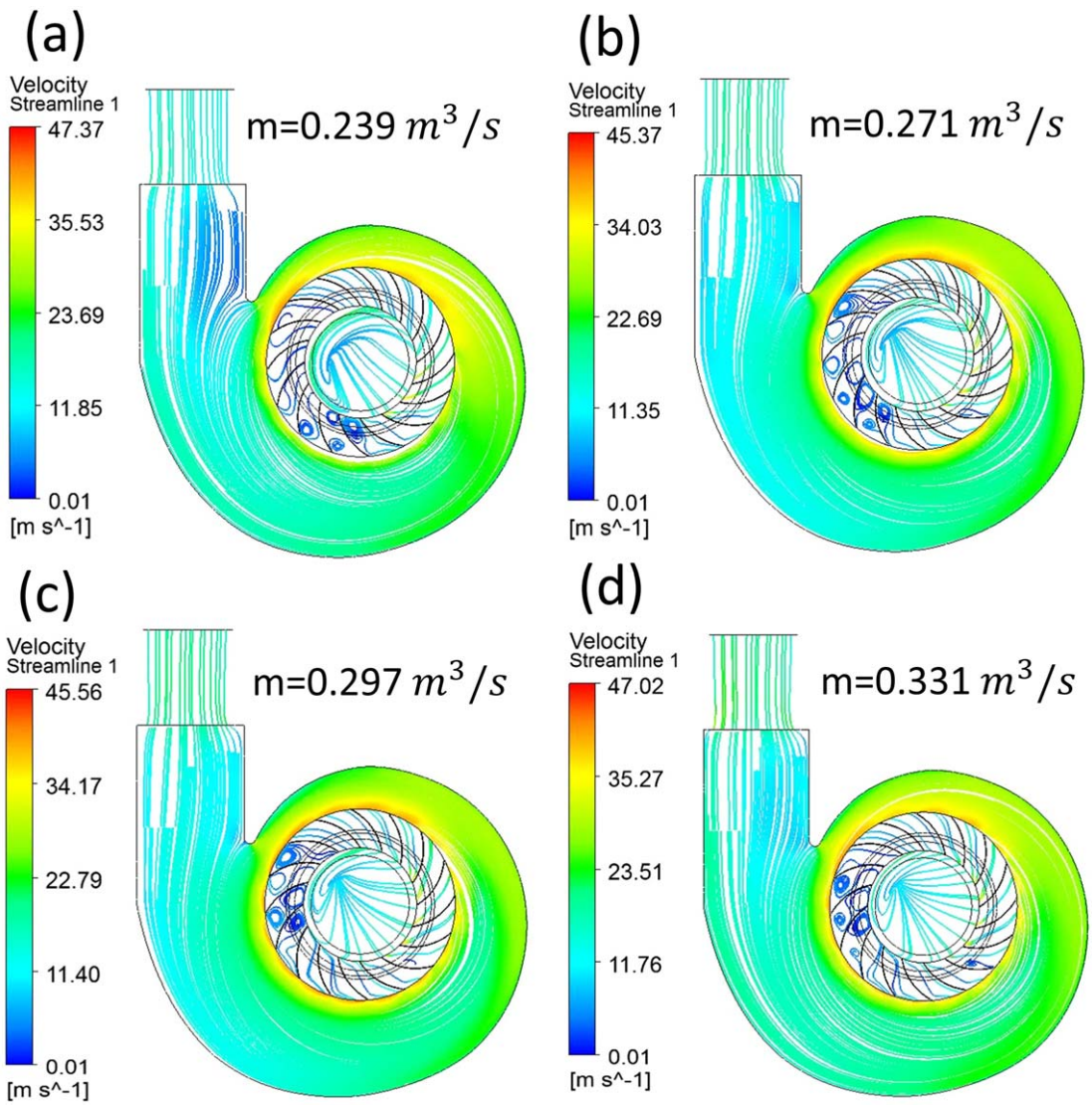

Figure 9. Velocity streamline contours at mid plane of casing for backward blade with variable mass flowrate.

The results of mesh 'c' seem optimized. Later, for grids 'd', 'e', and 'f', results showed negligible variation compared to mesh 'c' results. Hence, mesh 'c' is finalised for all further simulations to save time and cost of simulation.

The experimental and CFD studies are carried out with all three flow passages, i.e., backward, radial, and forward, are investigated at constant impeller speed with four mass flowrates. The flow diagram illustrates the work summary for experimental and CFD on flow behaviour and performance graphs for different cases, as shown in figure 5. Each experiment group was run with three repetitions to reduce random test errors, and the average value was calculated.

4. Results and discussions

The flow parameters for experimental and CFD analysis were calculated and compared after the measurement of static pressure, static pressure difference, total pressure difference, and flow velocity at the casing outlet with varying mass flow rates through backward, radial, and forward blade impellers. Additionally, experimental, and computational calculations were used to determine the efficiency of the centrifugal fan for all three blades.

Figures 6(a)–(d), 7(a)–(d), and 8(a)–(d) show the static pressure contour at the mid-plane of the casing from suction to exit for the backward, radial, and forward blade impellers, respectively, with four varying mass flow rates for each blade impeller at an impeller speed of 2800 rpm. The range of static pressure at the mid-plane casing for the backward blade (refer to figure 6) lies between 102798.14 Pa to 99525.30 Pa; for the radial blade

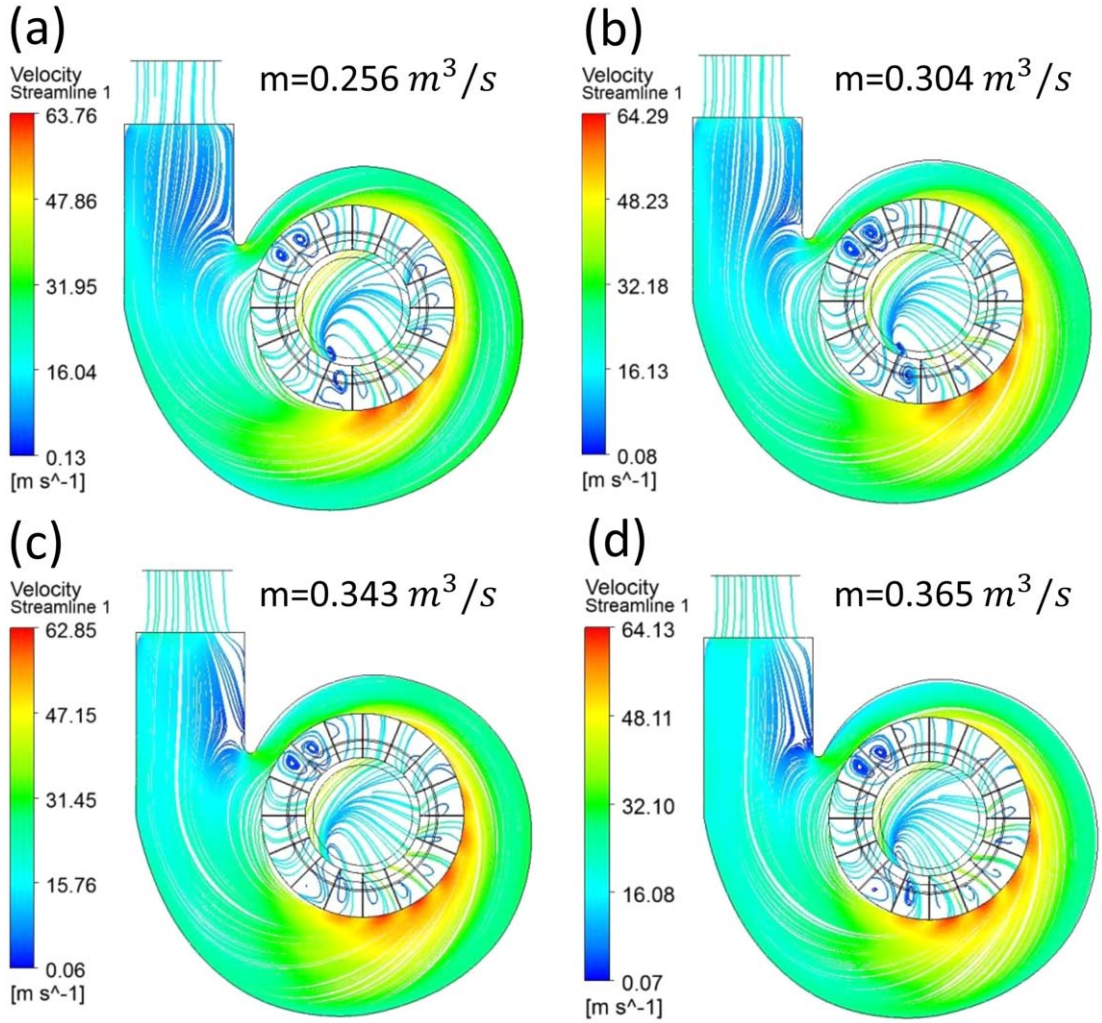

Figure 10. Velocity streamline contours at mid plane of casing for radial blade with variable mass flowrate.

(refer to figure 7), it is 103036.38 Pa to 99514.1 Pa; and for the forward blade (refer to figure 8), it is 104470.6 Pa to 99485.8 Pa, respectively.

From the static pressure range, it can be concluded that for the forward blade, the static pressure rise is higher than the radial and backward blade impellers of the centrifugal fan. Figures 6–8 show a static pressure rise from the tongue to the outlet of the casing and in the impeller. This rise in static pressure is due to the diffuser geometry of the casing and the generation of centrifugal force by the impeller. Also, the pressure perturbations are quite high near the tongue region. With reference to the flow rate, it can also be observed that the static pressure difference decreases as the flow rate increases. Furthermore, on the discharge side, there is a higher pressure, and on the suction side, there is a lower pressure on the impeller blade, which causes flow reversal, along with that decrease in static pressure in the volute casing because of the frictional wall loss. In addition to that flow separation occurs on the suction side of the impeller, and as a consequence, the static pressure in that region falls below atmospheric pressure.

Figures 9(a)–(d)–11(a)–(d) show the velocity streamline contours at the mid-plane of the casing for the backward, radial, and forward blade impellers, respectively, with four varying mass flow rates for each blade impeller at an impeller speed of 2800 rpm. The streamline shows the flow direction inside the impeller and volute casing of the centrifugal fan. The velocity range for the backward blade is 0.01 to 47.73 m s^{-1}; for the radial blade, it is 0.06 to 64.29 m s^{-1}; and for the forward blade, it is 0.03 to 85.55 m s^{-1}. For a constant speed of the impeller and an increase in mass flow rate, the minimum velocity is observed for the backward blade impeller and the maximum for the forward blade impeller of the centrifugal fan. Figures 9–11 show that the streamline distribution in the volute casing is uniform, strengthening the available volute casing design. However, reverse flow is observed inside the impeller. It was also observed that reverse flow inside the flow passage increased with an increase in mass flow rate. Compared to the forward and radial blade impellers, the streamline distribution is more uniform in the backward blade impeller (refer to figure 9). In the backward blade impeller, it is also

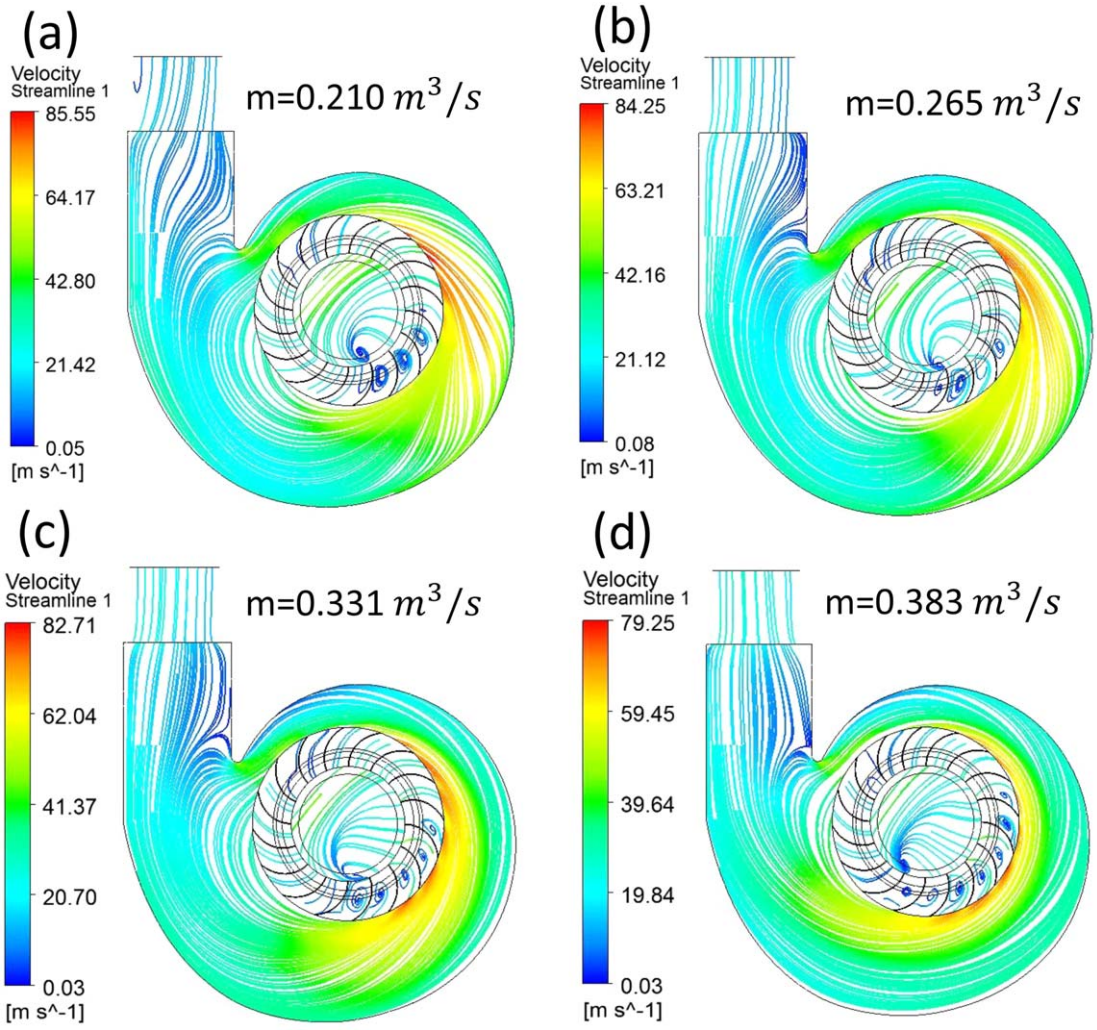

Figure 11. Velocity streamline contours at mid plane of casing for forward blade with variable mass flowrate.

observed that with the increase in mass flow rate, the reverse flow region shifts near to the tongue of the volute casing. The radial blade impeller reverse flow region remains as it is, with an increase in mass flow rate. Also, in the forward blade, the reverse flow remains as it is on the opposite side of the tongue of the volute casing with the increase in the mass flow rate.

It is observed that velocity is higher on the pressure side and lower on the suction side of the impeller blade due to the reverse flow inside the impeller blade passages, as shown in figures 9–10. The lower velocity observed in the impeller near the tongue of the casing is due to higher pressure fluctuations at the tongue region. The presence of vortices of varying degrees is also observed in all three cases. The streamline separation and vortices formation are different in all three categories of flow passages. This is one of the most probable reasons for the observed performance differences in the three categories of flow passages.

Figures 12(a)–(d), 13(a)–(d), and 14(a)–(d) indicate the static pressure contours on the blade surface for the backward, radial, and forward blade impellers of the centrifugal fan with four variable mass flow rates for each blade impeller at an impeller speed of 2800 rpm. The range of static pressure on the blade surface for the backward blade is 102850.05 Pa to 99450.54 Pa; for the radial blade, it is 103030.95 Pa to 99396.65 Pa; and for the forward blade, it is 103575.95 Pa to 98764.91 Pa.

From the range of static pressure on the blade surface, it is observed that higher static pressure is developed in the forward blade than in the radial and backward blade impellers of the centrifugal fan; this is due to the rise in static pressure from the inlet to the outlet of the impeller. As the air glides on the surface of the blades, there is a static pressure rise because the velocity head developed by the forward blade impeller is higher than the backward and radial blade impellers. Furthermore, it was seen that the static pressure is higher on the pressure side and lower on the suction side for all three types of impellers and that the highest pressure is at the tip of the blade for all three types.

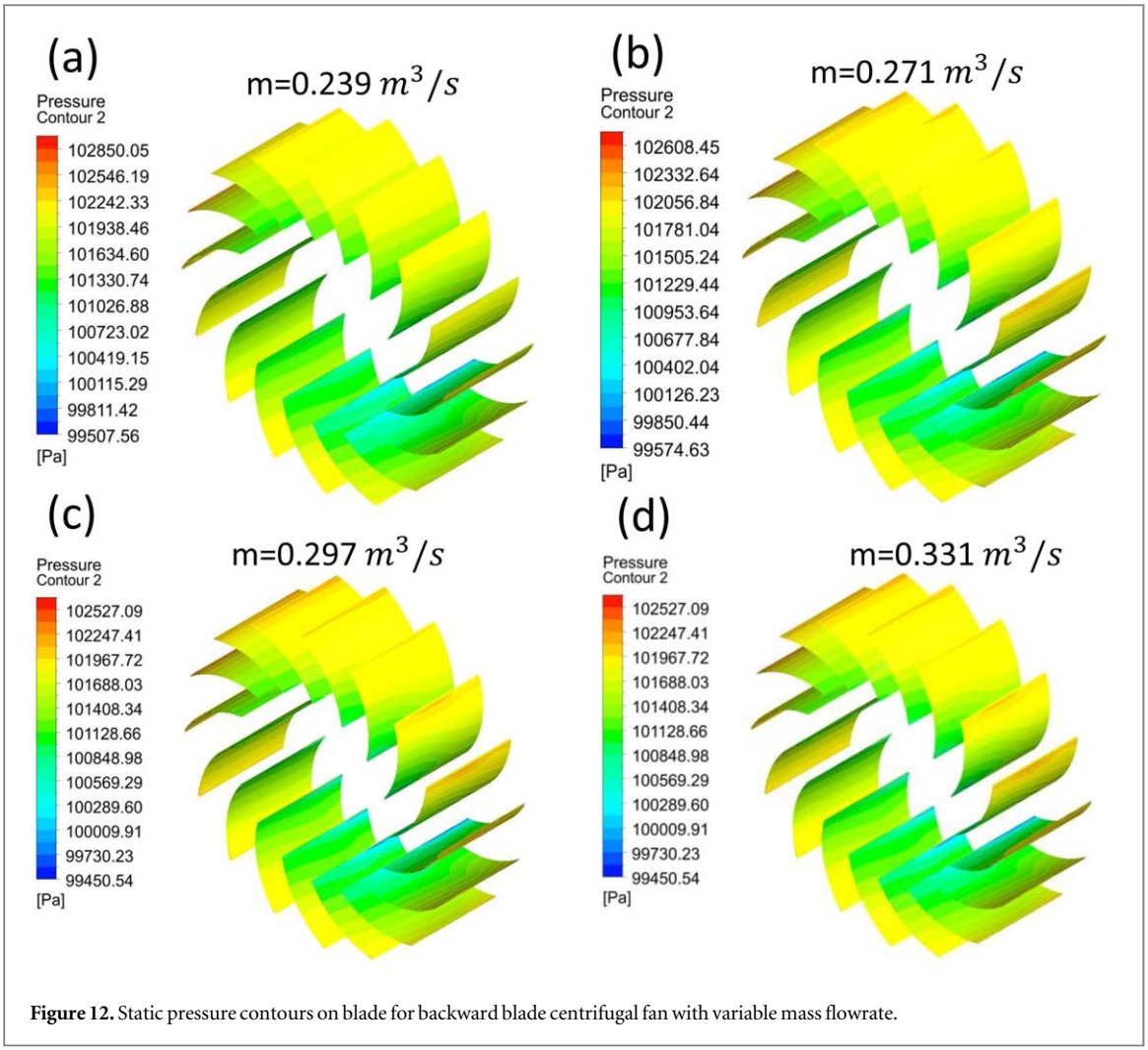

Figure 12. Static pressure contours on blade for backward blade centrifugal fan with variable mass flowrate.

Figures 15(a)–(c) shows the comparison of experimental and CFD results for a centrifugal fan with different impeller blade configurations, such as a backward blade, a radial blade, and a forward blade, for static pressure at the casing outlet with variable mass flowrates at an impeller speed of 2800 rpm. From figures 15(a)–(c), it can be observed that CFD results are marginally higher compared to the experimental results. This variation in the results can be due to losses like wall frictional loss, flow leakage loss, and obstructions like pressure measuring taping, sudden contraction and expansion in the cross-section, and a flow control valve. Numerical results overpredict the experimental data with an average absolute error of static pressure at the casing outlet by 2%, 10% and 23% for the backward, radial, and forward blade impellers, respectively.

Figures 16(a)–(c) compares the experimental and CFD findings for a centrifugal fan with various impeller blades (backward blade, radial blade, and forward blade) for the static pressure difference at the casing with varied mass flowrates at an impeller speed of 2800 rpm. Figures 16(a)–(c) indicates that a similar decreasing trend of the graph with reference to mass flow rate was obtained as that obtained for the static pressure. It also indicates that the CFD results are marginally higher than the experimental results. The numerical results overpredict the experimental data with an average absolute error of 4.58%, 6.5% and 19.1% for the backward, radial, and forward blade impellers, respectively. The error between CFD and experimental results for the forward blades is higher compared to the error for backward and radial blades. This high error in the case of forward blades is due to the flow behavior around the forward blades is more complex and unsteady compared to the backward and radial blades. This is because the forward blades have a curved shape that generates more vortices and flow separation regions, leading to more complex flow behavior. The numerical modeling of such complex flow behavior is more challenging and can result in higher errors compared to simpler flow behavior around the backward and radial blades and high level of turbulence generated due to the increasing mass flow rate in the flow passage of the fan. Also, the reverse flow region is higher compared to the radial and backward blade impellers of a centrifugal fan. From figures 16(a)–(c), it can be observed that the static pressure difference decreases with an increase in flow rate for all three impellers. It can also be observed that the static pressure difference at the casing decreases more in the backward blade than in the radial and forward blade impellers of

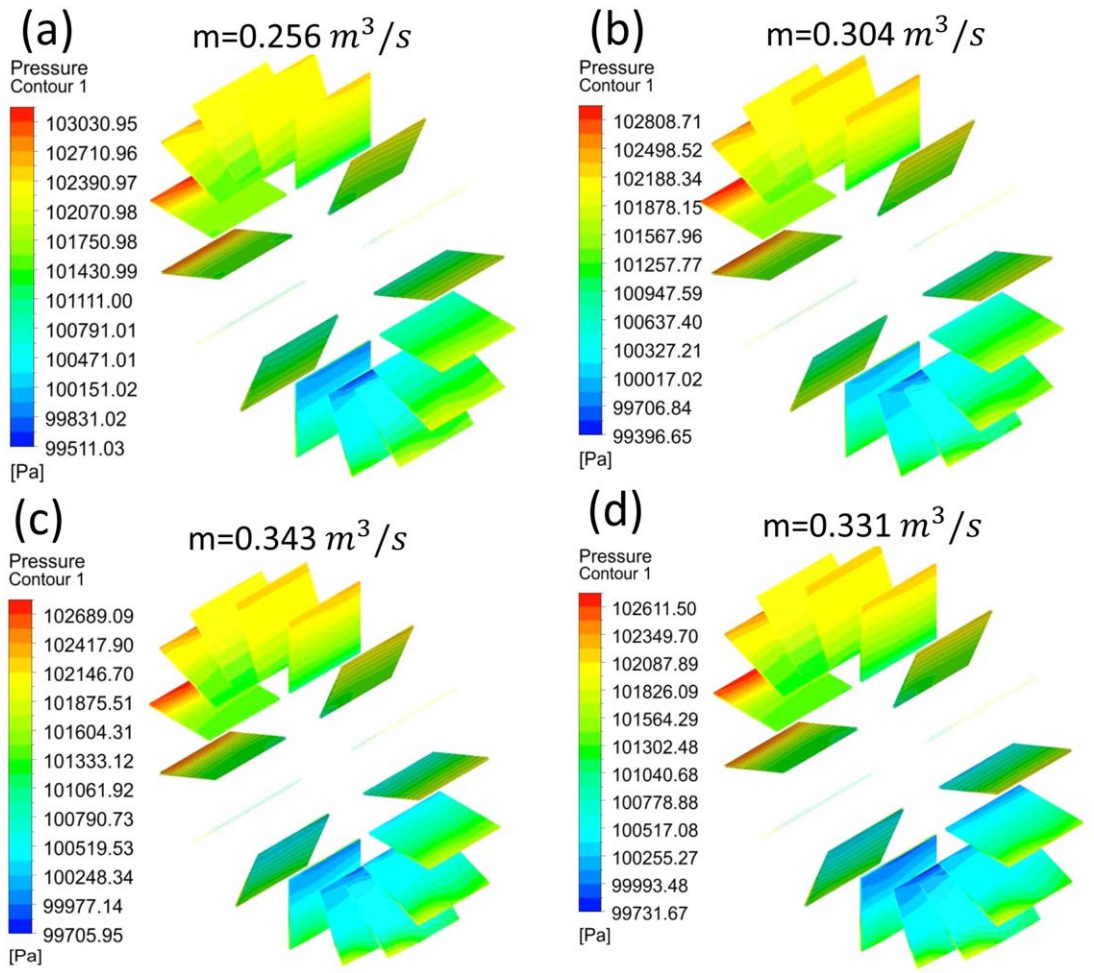

Figure 13. Static pressure contours on blade for radial blade centrifugal fan with variable mass flowrate.

the centrifugal fan, respectively. The forward blade has a greater increase in static pressure difference at the casing than the radial and backward blades. However, the static pressure difference at the casing is higher in the radial blade centrifugal fan than in the forward blade centrifugal fan because the geometrical parameters are different for the impeller with the same volute configuration.

Figures 17(a)–(c) compares the experimental and CFD findings for a centrifugal fan with a backward blade, radial blade, and forward blade impeller for the total pressure difference at the casing with varied mass flow rates at an impeller speed of 2800 rpm. From figures 17(a)–(c), it can be observed that the CFD results are only marginally higher compared to the experimental results. The numerical results overpredict the experimental data with an average absolute error of 4.92%, 7.4% and 22.8% for the backward, radial, and forward blade impellers, respectively. This higher deviation (22.8%) can be attributed to the higher level of turbulence in the forward blade impeller. The range of total pressure difference at the casing is higher for the forward blade impeller of the centrifugal fan than for the radial and backward blade impellers of the centrifugal fan. This is due to the absolute velocity of the forward blade impeller being higher than the radial and backward blade impellers of a centrifugal fan. Similarly, the total pressure difference at the casing decreases more rapidly for a constant speed of the backward blade impeller than the radial and forward blade impellers of the centrifugal fan.

Figures 18(a)–(c) shows the comparison of experimental and CFD results for a centrifugal fan with different impeller blade configurations, such as a backward blade, a radial blade, and a forward blade, for the velocity at the outlet of the casing with variable mass flowrates at an impeller speed of 2800 rpm. The results suggest that the CFD results are very much in tune with the experimental results. For the backward, radial, and forward blade impellers, the absolute differences between the CFD and experimental results were 1.67%, 8.53%, and 4.5%, respectively, which made the computational model used in the CFD more accurate.

Figures 19(a)–(c) compares the experimental and CFD findings for a centrifugal fan with a backward blade, radial blade, and forward blade impeller for efficiency with varied mass flow rates at an impeller speed of 2800 rpm. It can be observed that the CFD results are slightly higher compared to the experimental results. This variation in the results can be due to losses like wall frictional loss, flow leakage loss, and obstructions like

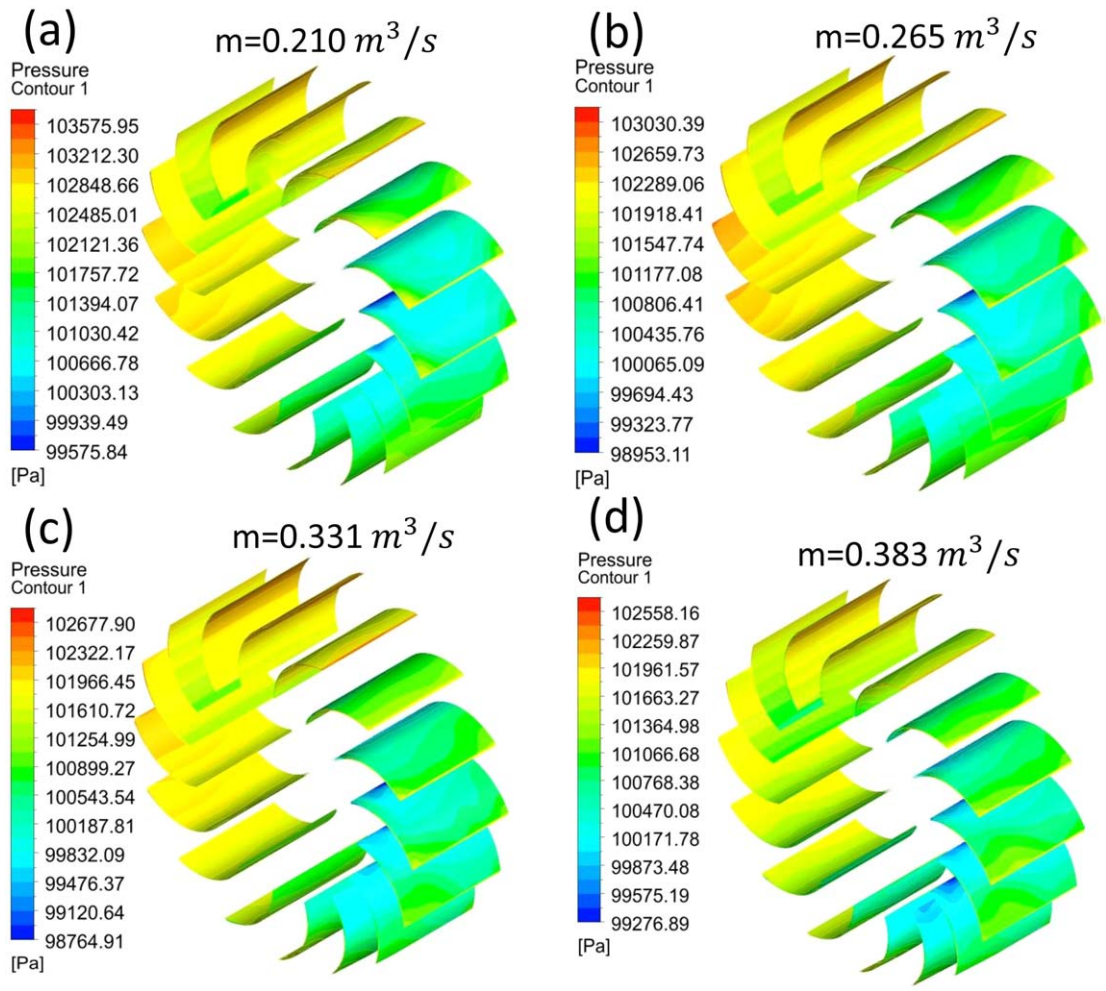

Figure 14. Static pressure contours on blade for forward blade centrifugal fan with variable mass flowrate.

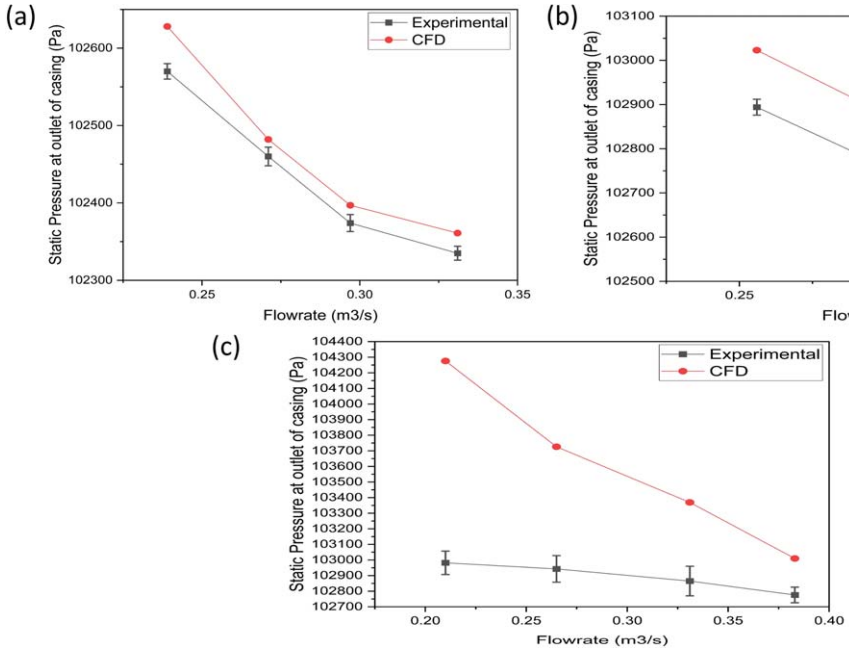

Figure 15. Experimental and CFD results of a centrifugal fan for static pressure at outlet of casing with variable mass flowrate: (a) Backward blade, (b) Radial blade, (c) Forward blade.

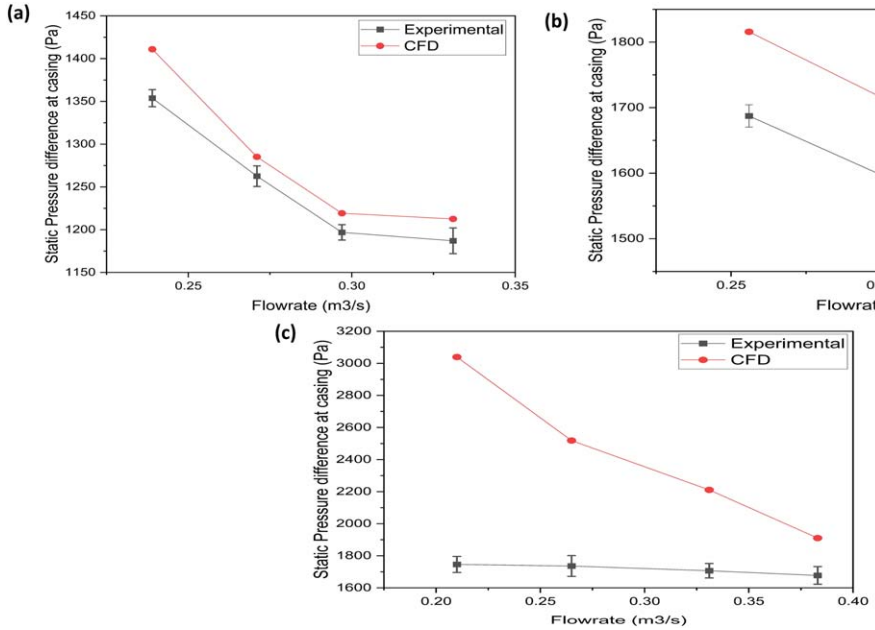

Figure 16. Experimental and CFD results of a centrifugal fan for static pressure difference at casing with variable mass flowrate: (a) Backward blade, (b) Radial blade, (c) Forward blade.

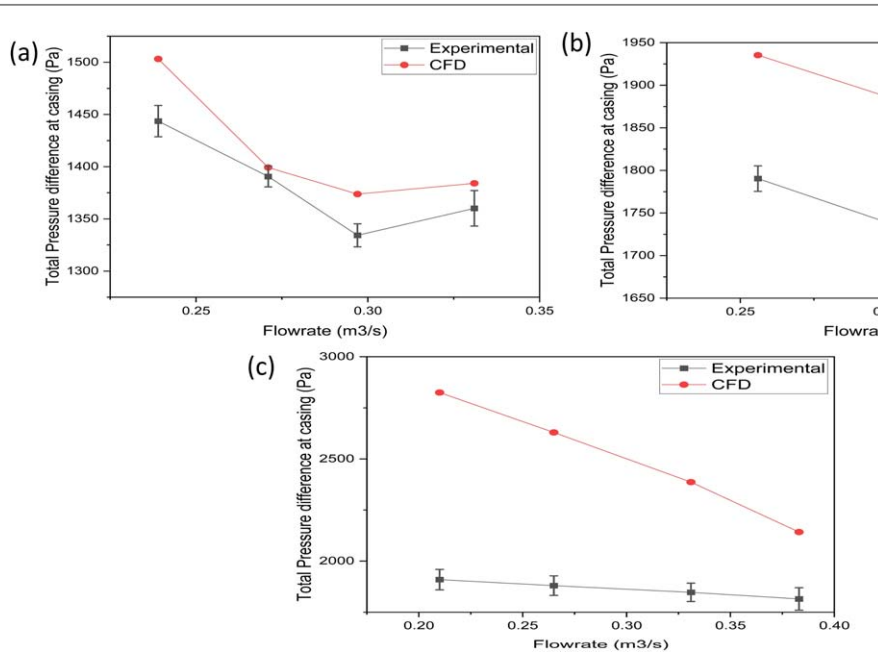

Figure 17. Experimental and CFD results of a centrifugal fan for total pressure difference at casing with variable mass flowrate: (a) Backward blade, (b) Radial blade, (c) Forward blade.

pressure measuring taping, sudden contraction and expansion in the cross-section, and a flow control valve. The numerical results overpredict the experimental data with an average absolute error of stagnation efficiency of 4.92%, 7.4%, and 22.8% for the backward, radial, and forward blade impellers, respectively. As shown in figures 19(a)–(c), the calculated efficiency obtained from the experiments suggests a linear increase in efficiency with an increase in flow rate for three impellers with the same volute configuration for a forward, radial, and backward blade centrifugal fan. These characteristic curves are quite in tune with the available literature, which again strengthens the accuracy of the experimental results. The maximum efficiency of 76.07% is obtained for the backward blade. Though the total pressure difference at the casing is lower for the backward blade, the efficiency for the backward blade is higher compared to the other two blades. The reason was justified

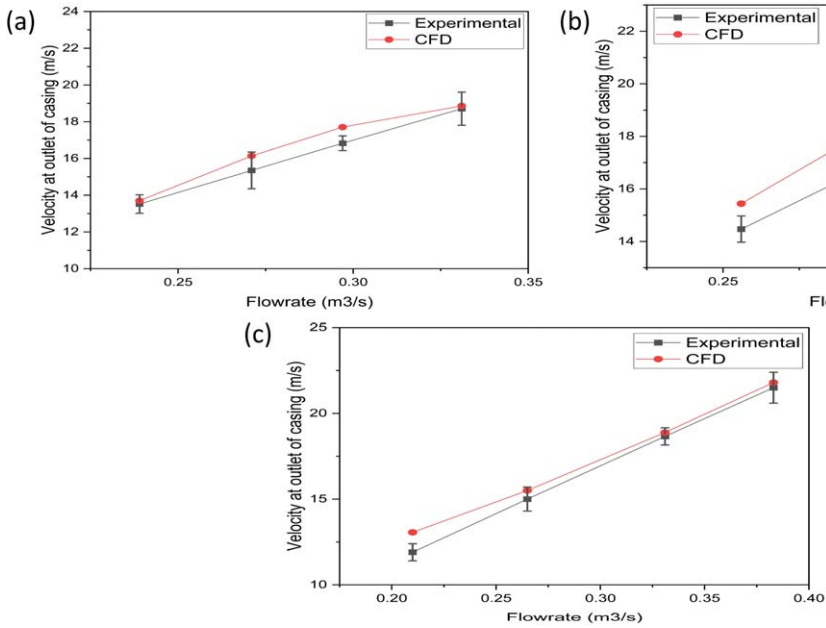

Figure 18. Experimental and CFD results of a centrifugal fan for velocity at outlet of casing with variable mass flowrate: (a) Backward blade, (b) Radial blade, (c) Forward blade.

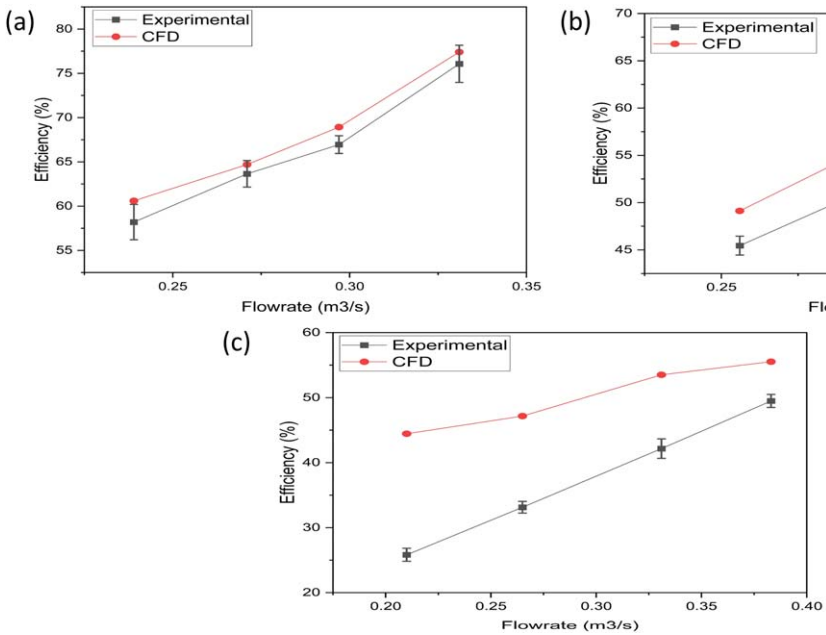

Figure 19. Experimental and CFD results of a centrifugal fan for efficiency with variable mass flowrate: (a) Backward blade, (b) Radial blade, (c) Forward blade.

experimentally, as the power required for operating the fan was also lower compared to the other two impeller blades.

5. Conclusion

The exhaustive numerical and experimental studies carried out on the influence of flow passages in nearly identical sized backward, radial, and forward blade impellers within the same volute configuration leads to the following conclusions:

- Pressure pulsations are observed at the impeller outlet near the tongue region, caused by obstruction of the tongue. Hence the design of the tongue is critical in fan design to reduce back flow and recirculation.
- The flow phenomenon of recirculation near the tongue region is confirmed by numerical analysis, as shown by the velocity streamline diagram. The jets and wakes were observed in the vicinity of the tongue region.
- A blade's low and high-pressure regions along the suction and pressure sides were visualised by numerical analysis. Pressure and velocity contours within the blade passage also confirm energy transfer from the impeller to the fluid.
- The turbulence generated for the forward blade flow passage is higher than the radial and backward blade flow passages.
- The efficiency of the backward blade impeller is relatively higher compared to the radial and forward blade impellers. Also, there was an increase in efficiency with the rise in the mass flow rate.

Acknowledgments

The authors thank the Department of Mechanical Engineering, Sardar Vallabhbhai National Institute of Technology, Surat for provision of research facilities for the present work.

Data availability statement

All data that support the findings of this study are included within the article (and any supplementary files).

ORCID iDs

Abhimanyu Chaudhari https://orcid.org/0000-0002-7737-9544
Vikas Diwakar https://orcid.org/0000-0001-7257-8168

References

[1] Kim B *et al* 2022 Optimization of centrifugal pump impeller for pumping viscous fluids using direct design optimization technique **10** 774
[2] Singh O P, Khilwani R, Singh O P, Sreenivasulu T and Kannan M 2011 Parametric study of centrifugal fan performance: experiments and numerical simulation *researchgate.net* **33** 33–50 Accessed: Dec. 23, 2022. [Online]. Available: https://researchgate.net/profile/Rakesh-Khilwani-2/publication/267971543_PARAMETRIC_STUDY_OF_CENTRIFUGAL_FAN_PERFORMANCE_EXPERIMENTS_AND_NUMERICAL_SIMULATION/links/570c36e808ae2eb94223beaa/PARAMETRIC-STUDY-OF-CENTRIFUGAL-FAN-PERFORMANCE-EXPERIMENTS-AND-NUMERICAL-SIMULATION.pdf
[3] Ayad A and Abdalla H … A A E-A-I C on, and undefined 2014, '3-D numerical study of the effect of impeller blades slot on the centrifugal pump performance using CFD,' *journals.ekb.e.g.*, Accessed: Dec. 23, 2022. [Online]. Available https://journals.ekb.e.g./article_35605_800cc96fed8407a377f087737afcae21.pdf
[4] Bhope D V and Padole P M 2004 Experimental and theoretical analysis of stresses, noise and flow in centrifugal fan impeller *Mech. Mach. Theory* **39** 1257–71
[5] Bachtiar A, Pohan A and Ervil R N N-I J of, and undefined 2021, 'Effect of Geometric differences impeller blades on performance blower as turbine (BAT) on pico-hydro scale,' *ijrer.org*, Accessed: Dec. 23, 2022. [Online]. Available: https://ijrer.org/ijrer/index.php/ijrer/article/view/11943
[6] Korkmaz E, Gölcü M and Kurbanoğlu C 2017 Effects of blade discharge angle, blade number and splitter blade length on deep well pump performance *J. Appl. Fluid Mech.* **10** 1735–3645
[7] Zinchenko A *et al* 2021 Materials selection and design options analysis for a centrifugal fan impeller in a horizontal conveyor dryer *Materials* **14** 6696
[8] Wright T, Madhavan S and DiRe J 1983 Centrifugal fan performance with distorted inflows *Am. Soc. Mech. Eng.* (https://doi.org/10.1115/83-jpgc-gt-5)
[9] Lei Z, Rui W, Wei Y and Songling W 2015 Simulation of air jets for controlling stall in a centrifugal fan *Proc. Inst. Mech. Eng. Part C J. Mech. Eng. Sci.* **229** 2045–55
[10] Choi M, Smith N H S and Vahdati M 2012 Validation of numerical simulation for rotating stall in a transonic fan *J. Turbomach.* **135** 1–8
[11] Shojaeefard M H, Salimian Rizi B, Khalkhali A and Tahani M 2015 A new method to calculate centrifugal pump performance parameters for industrial oils, *Jafmonline.Net* **8** 673–81
[12] Farid A, Hassan A, Abdalla H M, Abo A S and Aly E-A Effect of impeller blade slot on centrifugal pump performance,' *engineeringresearch.org*, 2016, Accessed: Dec. 23, 2022. [Online]. Available: https://engineeringresearch.org/index.php/GJRE/article/view/1498
[13] Szpicer A, Bińkowska W, Wojtasik-Kalinowska I, Salih S M and Półtorak A 2023 Application of computational fluid dynamics simulations in food industry *Eur. Food Res. Technol.* (https://doi.org/10.1007/s00217-023-04231-y)
[14] Chaudhari A, Sharma A, Awale A S, Khan Yusufzai M Z and Vashista M 2022 Modeling and simulation study of dry ultrasonic vibration-assisted grinding of tool steel with single alumina abrasive grit *J. Manuf. Sci. Eng.* **144** 1–32
[15] Bhatti M M, Marin M, Zeeshan A and Abdelsalam S I 2020 Editorial: recent trends in computational fluid dynamics *Front. Phys.* **8** 1–4

[16] Kozelkov A S, Kurulin V V, Lashkin S V, Shagaliev R M and Yalozo A V 2016 Investigation of supercomputer capabilities for the scalable numerical simulation of computational fluid dynamics problems in industrial applications *Comput. Math. Math. Phys.* **56** 1506–16
[17] Mader C A, Kenway G K W, Yildirim A and Martins J R R A 2020 ADflow: an open-source computational fluid dynamics solver for aerodynamic and multidisciplinary optimization *J. Aerosp. Inf. Syst.* **17** 508–27
[18] Moczko P *et al* 2022 Enhancing efficiency of industrial centrifugal fans using blade adjustment mechanism *Energies* **15** 1–15
[19] Lv H, Yang W and Zhang W J 2022 Numerical simulation and analysis of the aerodynamic noise of a nautilus-inspired bionic multiblade centrifugal fan *J. Mech. Sci. Technol.* **36** 4475–89
[20] Amrit A, Leifsson L and Koziel S 2018 Multi-fidelity aerodynamic design trade-off exploration using point-by-point Pareto set identification *Aerosp. Sci. Technol.* **79** 399–412